Journal of Alloys and Compounds 509 (2011) 3894–3898

Contents lists available at ScienceDirect

Journal of Alloys and Compounds

journal homepage: www.elsevier.com/locate/jallcom

Fabrication of Pd–Fe nanowires with a high aspect ratio by AAO template-assisted electrodeposition

Nevin Taşaltın[a], Sadullah Öztürk[a], Necmettin Kılınç[a], Hayrettin Yüzer[b], Zafer Ziya Öztürk[a,b,*]

[a] Gebze Institute of Technology, Science Faculty, Department of Physics, 41400 Gebze, Kocaeli, Turkey
[b] TUBITAK Marmara Research Center, P.O. Box 21, 41470 Gebze, Kocaeli, Turkey

ARTICLE INFO

Article history:
Received 7 October 2010
Received in revised form
15 December 2010
Accepted 19 December 2010
Available online 28 December 2010

Keywords:
Pd–Fe alloy
Nanowire
Electrodeposition
Nucleation
AAO template

ABSTRACT

In this study, vertically oriented $Pd_{0.86}Fe_{0.14}$ nanowires have been fabricated using an anodized aluminum oxide (AAO) template by direct voltage electrodeposition at room temperature. AAO template-assisted electrodeposition of Pd–Fe was carried out in $Pd(NH_3)_2Cl_2$:$FeSO_4 \cdot 7H_2O$ solution. The AAO template and the $Pd_{0.86}Fe_{0.14}$ nanowires were characterized by scanning electron microscopy (SEM), energy dispersive X-ray (EDX) methods and X-ray diffraction (XRD). It was observed that the $Pd_{0.86}Fe_{0.14}$ nanowires were approximately 65 nm in diameter and 10 μm in length with an aspect ratio of 153 in a relatively large area of about 4 cm^2. The nucleation rate and the number of atoms in the critical nucleus are determined from the analysis of current transients.

1. Introduction

Metal nanostructures, such as nanoparticles, nanowires and nanoarrays have attracted much attention in recent years due to their extraordinary electronic, magnetic, optic and chemical properties [1–3]. The controllable growth of metal nanowires has been a topic of continuing investigation because of the need to obtain high-performance and high-density nanoelectronic devices, such as magnetic recording devices, solar cells, hydrogen storage devices, transistors, chemical sensors, and so forth [4–8]. Over the last several years, metal nanowire arrays have been fabricated using a variety of techniques, such as electrochemical methods, chemical vapor deposition, sol–gel and template assisted electrodeposition [5–8]. Recently, the template-assisted fabrication of functional nanowires has attracted considerable attention. This is mainly owing to the possibility of controlling the length, diameter, and density of the fabricated nanowires by varying the template and/or deposition parameters. The template method has been accomplished using a variety of templates, such as polycarbonate templates (PC), nanochannel alumina (NCA) and anodized aluminum oxides (AAO). It has been considered that the AAO template is an ideal template as it possesses many desirable characteristics, including tunable pore dimensions, good mechanical strength, thermal stability and ordered nanotubes at a high density (10^9–10^{11} cm^2) [9–11]. Furthermore, the distribution patterns of pore size in the AAO template can directly influence the diameters of the nanowires, which can be easily controlled by varying the preparation conditions of the AAO, such as the temperature and oxidation voltage. Thus, it is also a useful technique for the deposition of metals with different sizes.

The fabrication of Fe–Pd alloy nanowires is very interesting to study both in terms of the magnetic properties and the martensitic transformation on the nano scale [12]. Also, high uniaxial anisotropy also enables Fe–Pd particles to overcome thermal fluctuations even for very small sizes. Moreover, the Fe–Pd alloy exhibits the properties of the shape memory effect (SME) and the magnetostrictive effect caused by face-centered cubic (fcc) to face-centered tetragonal (fct) thermoelastic martensitic transformation [13–15]. On the other hand, one-dimensional nanostructured Pd–Fe alloys have attracted extensive attention recently because of their physical and chemical properties; they are considered to be promising candidate materials for room temperature hydrogen sensing because they have good physio-mechanical strength and resistance to poisoning by other chemical species. Baba et al. [16] studied the interaction of Pd and Pd alloys with hydrogen gas and found that the electrical resistance of Pd and Pd alloys was dependent on the absorbed hydrogen amount of the metal phase. Although Pd and Pd alloys as H_2 sensing materials were reported

* Corresponding author at: Gebze Institute of Technology, Science Faculty, Department of Physics, Cayirova Campus, Istanbul St. no. 101, 41400 Gebze, Kocaeli, Turkey. Tel.: +90 2626051306; fax: +90 2626538490.
E-mail address: zozturk@gyte.edu.tr (Z.Z. Öztürk).

0925-8388/$ – see front matter © 2010 Elsevier B.V. All rights reserved.
doi:10.1016/j.jallcom.2010.12.153

by many research groups [17–23], further improvement is still required with respect to selectivity, sensitivity and the lifetime of the sensors. To date, only a limited number of reports describing the fabrication of Fe–Pd alloy nanowires has appeared in the literature [12,24–26], and there is no report about the fabrication of Pd–Fe nanowires which have low percentage of Fe content. Fei et al. [12] fabricated $Fe_{0.3}Pd_{0.7}$ and $Fe_{0.6}Pd_{0.4}$ nanowire arrays in 20 nm diameters by alternating current electrodeposition into an AAO template for the investigation of structural and magnetic properties. Then, Hu et al. [25] fabricated an AAO template approximately 60 nm in diameter and 40 μm in length. Afterwards, they fabricated a Fe–Pd nanowire array by dc electrodeposition using $FeCl_2$ and $PdCl_2$ with a pH value of three. Thus, $Fe_{0.95}Pd_{0.05}$ nanowires were fabricated for magnetic applications. Furthermore, Prida et al. [26] fabricated $Fe_{0.7}Pd_{0.3}$ nanowires approximately 35 nm in diameter and 4 μm in length using an AAO template by using alternating pulsed electrodeposition. When a chlorinated solution is used for electrodeposition (for instance, $FeCl_2$), the AAO template can be deformed or dissolved due to the high acidic media and pH value, unfortunately. Further studies and the development of the AAO template-assisted fabrication of nanowires are obviously of significant importance; however, there is an important lacking point in the literature about the fabrication of vertically free-standing Pd–Fe nanowires. Therefore, in this study, the fabrication of a Pd–Fe nanowire array with a high aspect ratio was reported in detail. Moreover, we reported new impressive results on the mechanism and kinetics of the initial stages of Pd–Fe electrodeposition in the AAO template, nucleation and growth kinetics of the Pd–Fe nanowires.

2. Experimental

AAO templates were fabricated by the two-step anodization of high-purity aluminum foils in 0.3 M oxalic acid solution under a constant dc voltage of 40 V [27,28]. A thin gold film was evaporated onto one surface of the as-prepared AAO template, which serves as the working electrode that has a silver epoxy attached to the Ti foil as a substrate. The used Ti foil was polished and cleaned beforehand. Then, the remaining aluminum of the AAO template, which was on the opposite side of the Au film, was etched in 5 wt% $HgCl_2$ for complete removal. After that, the AAO template was treated again in a 5 wt% phosphoric acid solution at 35 °C for 18 min to remove the AAO barrier layer. A schematic diagram of the preparation stages of the AAO template is given in Fig. 1.

Electrodeposition was carried out in a $Pd(NH_3)_2Cl_2$:$FeSO_4{\cdot}7H_2O$ solution with a pH value of six. Firstly, the $Pd(NH_3)_2Cl_2$ solution was prepared. $PdCl_2$ was added to hydrochloric acid and mixed until it completely dissolved the solution and it became brown and transparent. Pink-colored $Pd(NH_3)_2Cl_2$ appeared when the solution was dropped into dilute ammonia. The solution was stirred at 70 °C for 1 h. Then, the pH value of the solution was adjusted to seven by the addition of dilute sulfuric acid. Thus, the $Pd(NH_3)_2Cl_2$ solution was obtained. After that, we added $FeSO_4{\cdot}7H_2O$ and $C_7H_6O_6S{\cdot}2H_2O$ to the $Pd(NH_3)_2Cl_2$ solution and adjusted its pH value to about six by adding dilute ammonia. Finally, the Pd–Fe electrolyte was obtained.

Electrodeposition was carried out at room temperature (25 °C) using a three-electrode potentiostatic system with a saturated calomel electrode as a reference electrode and a graphite counter electrode. Pd–Fe was deposited using a potential of −1 V with a 1800-s deposition time by the direct voltage electrodeposition method. Then, the sample was annealed at 500 °C for 1.5 h. The annealing process provides Pd–Fe nanowires with a crystalline structure. To obtain free-standing Pd–Fe nanowires, the AAO template was dissolved with a dilute NaOH solution, and then carefully rinsed away with deionized water.

Scanning electron microscopy, energy dispersive X-ray (SEM; EDX, Jeol JSM 6335) methods and X-ray diffraction (XRD, Cu Kα, λ = 0.154 nm) were used to study the crystalline structure and morphologies of the fabricated Pd–Fe nanowires.

3. Results and discussion

The morphologies of the fabricated AAO template and the Pd–Fe nanowires were studied by SEM. Fig. 2a shows SEM image of the fabricated AAO template after the second anodization process. According to the SEM image, the fabricated hexagonally straight AAO nanotubes were approximately 70 nm in diameter, 10 μm in length, and had 90-nm interpore distances and an aspect ratio of 153. The AAO nanotube density is approximately 1.75×10^{14} cm^{-2} [27]. Fig. 2b shows the bottom of the AAO template after Al is removed with $HgCl_2$, and Fig. 2c shows the opened AAO barrier layer of template in phosphoric acid solution. It is clearly seen from comparison of Fig. 2a and c that the pore diameters of template are approximately same. So, the complete removal of the oxide barrier layer from the pore bottom of AAO is succeeded.

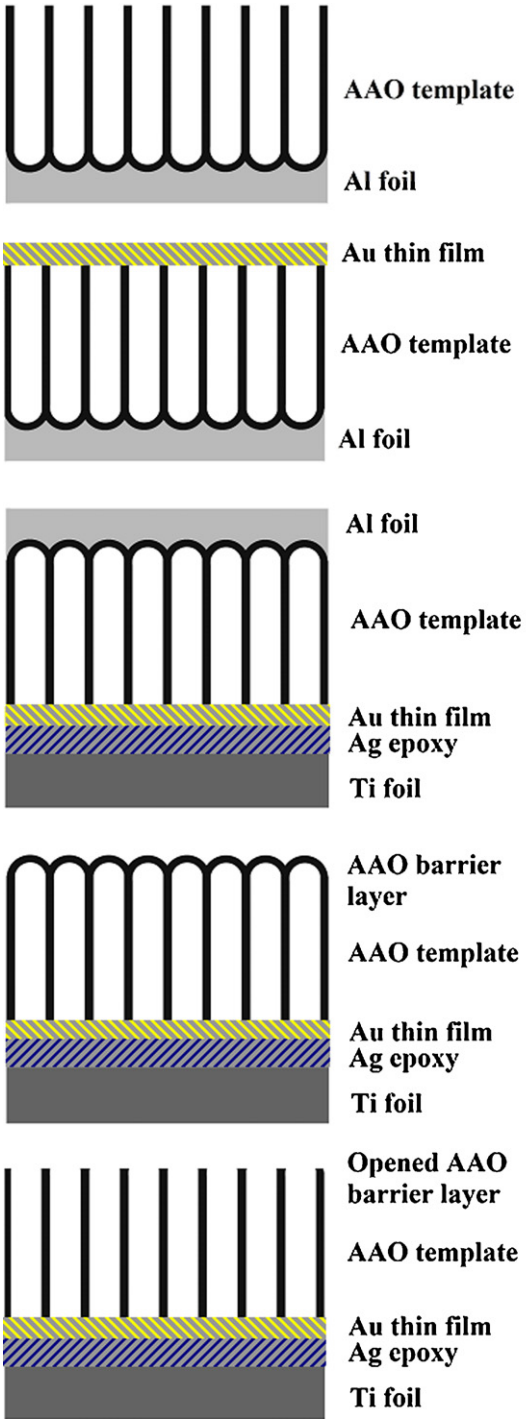

Fig. 1. Schematic diagram of the preparation stages of the AAO template.

Fig. 3 shows the current behavior as a function of potential during the electrodeposition of the Pd–Fe nanowires.

Electrodeposition was carried out in a $Pd(NH_3)_2Cl_2$:$FeSO_4{\cdot}7H_2O$ solution with a pH value of six. Firstly, the $Pd(NH_3)_2Cl_2$ solution was prepared by adding $PdCl_2$ into hydrochloric acid and mixing

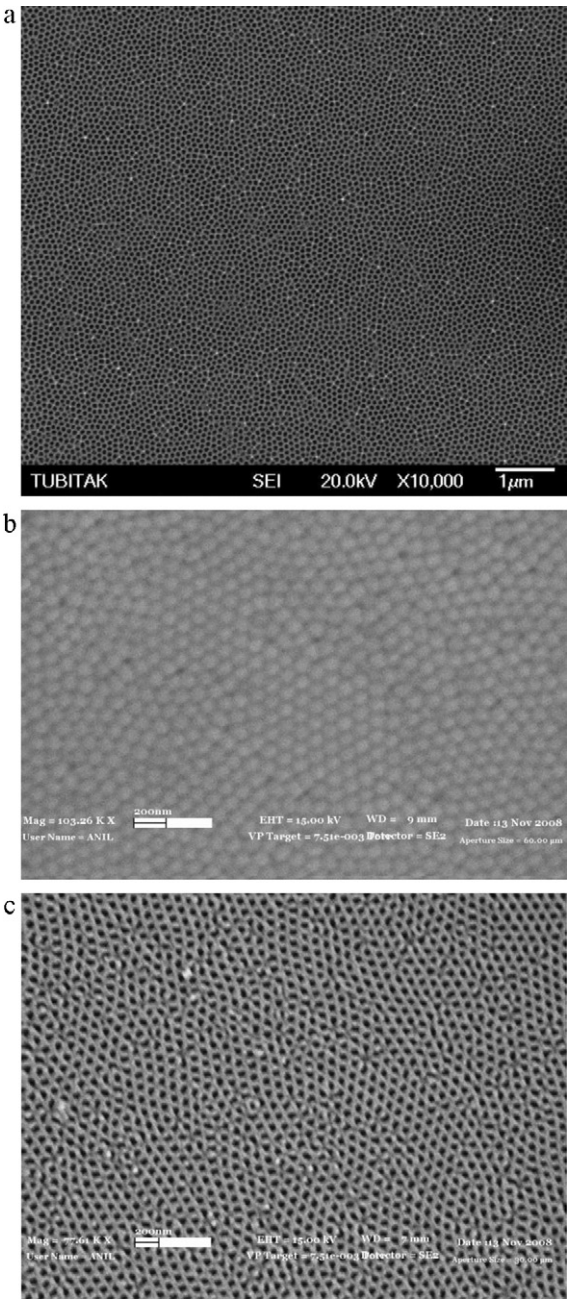

Fig. 2. SEM images of the fabricated AAO template: (a) top view, (b) bottom view, and (c) after removing of the alumina barrier layer.

it until the solution was completely dissolved and became brown and transparent as the following reaction shows:

$$PdCl_2 + HCl \rightarrow [PdCl_4]^{2-} + 2H^+ \quad (1)$$

Pink-colored $Pd(NH_3)_2Cl_2$ appeared when the solution was dropped into dilute ammonia as follows:

$$[PdCl_4]^{2-} + 4NH_3 \rightarrow [Pd(NH_3)_4]^{2+}Cl_2 \quad (2)$$

The solution was stirred at 70 °C for 1 h. Then, the pH value of the solution was adjusted to seven by the addition of dilute sulfuric acid as follows:

$$[Pd(NH_3)_4]Cl_2 + H_2SO_4 \rightarrow [Pd(NH_3)_2]Cl_2 + (NH_4)_2SO_4 \quad (3)$$

The $(NH_4)_2SO_4$ increases the electroconductivity of the electrodeposition solution. Thus, the $Pd(NH_3)_2Cl_2$ solution was

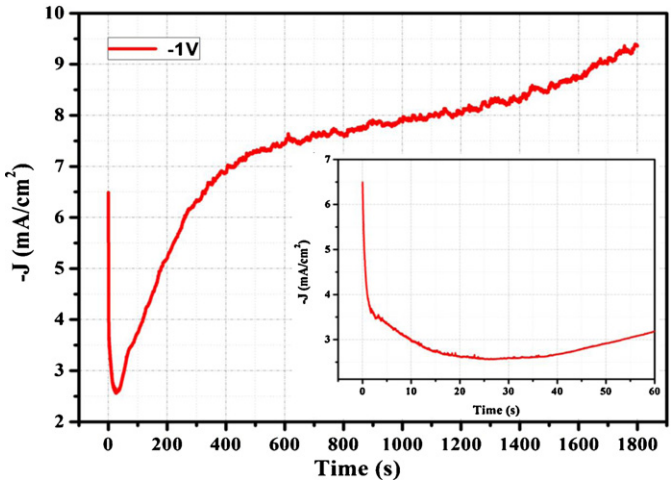

Fig. 3. The current transient during the electrodeposition of Pd–Fe in the AAO template.

obtained. After that, we dissolved $FeSO_4{\cdot}7H_2O$ and $C_7H_6O_6S{\cdot}2H_2O$ into three containers of distilled water and mixed that with a $Pd(NH_3)_2Cl_2$ solution and adjusted its pH value to about six by adding dilute ammonia. Finally, the Fe–Pd electrolyte was obtained.

The role of $C_7H_6O_6S{\cdot}2H_2O$ in electrodeposition is to prevent Fe^{2+}, from forming into Fe^{3+}. In previous studies, the electrodepo-

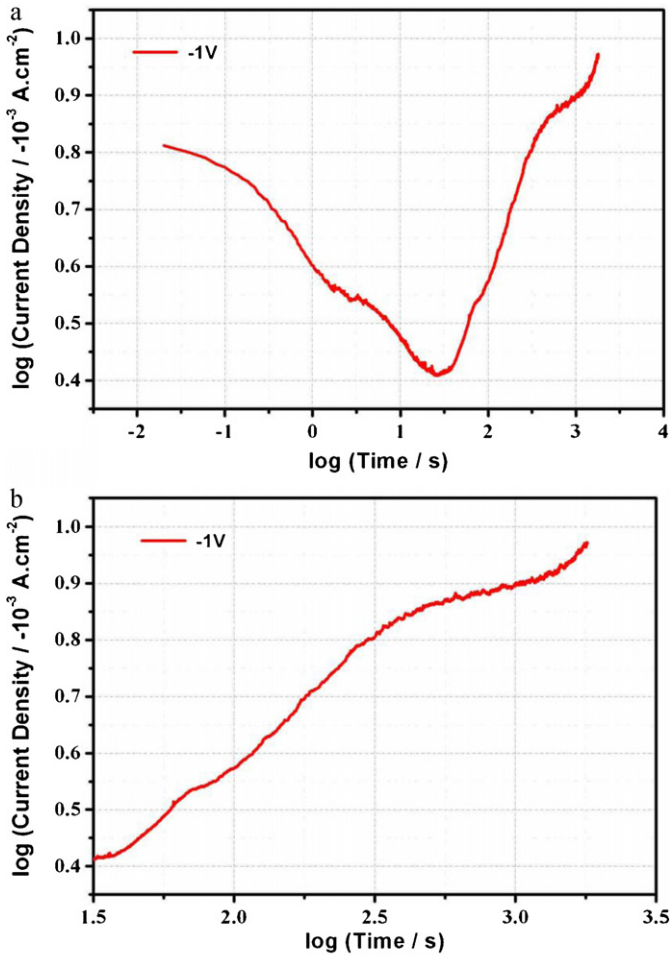

Fig. 4. Log(current density)–log(time) transients of increasing current density during Pd–Fe electrodeposition on the Au electrode.

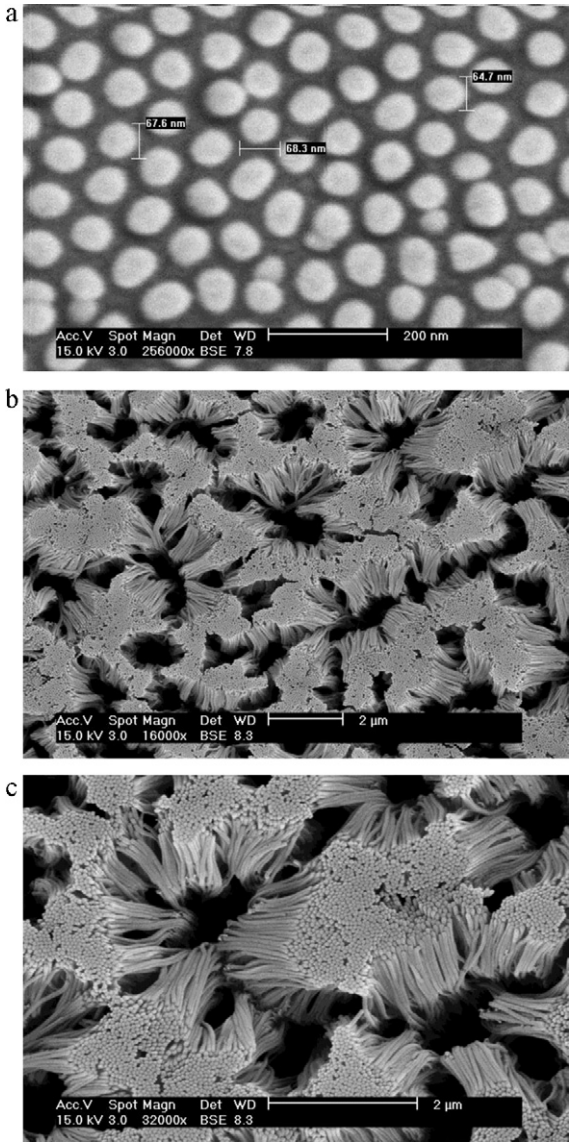

Fig. 5. (a) High magnification SEM image of the Pd–Fe nanowires in the AAO template. (b) SEM image of the Pd–Fe nanwires after removing the AAO template. (c) High magnification top view of the Pd–Fe nanowires.

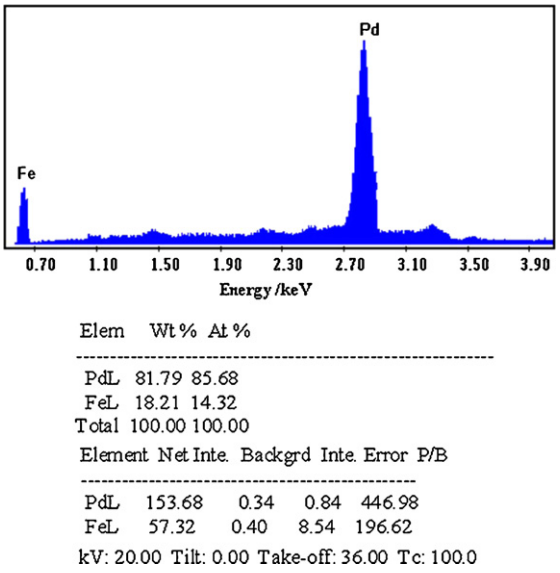

Fig. 6. EDX spectra from the surface of the as-deposited Pd–Fe nanowire array.

sition performed for equal molar Pd and Fe and for the Fe/Pd ratio in fabricated nanowires was up to 25%. In this study, for the electrodeposition of low ferric Fe^{2+} (<20) consisting of the Pd–Fe alloy, it easier to form the metal phase than a Pd^{2+} ion. Instead of equal molar Pd and Fe amounts, we used an electrolyte that consists of twice as little Fe^{2+} molarity in proportion to Pd^{2+} molarity. When voltage is applied the number of $[Pd(NH_3)_2]^{2+}$ ions in proportion to the number of the Fe^{2+} ions at the cathode are two times higher. The Fe ratio in the formed alloy is low, as expressed below:

$$[Pd(NH_3)_2] + 2e^- \rightarrow Pd^0 + 2NH_3 \quad (4)$$

$$Fe^{2+} + 2e^- \rightarrow Fe^0 \quad (5)$$

As shown in Fig. 3, the electrodeposition of the Pd–Fe nanowires is not a steady state process. According to the Pd–Fe and Au interaction, the current–time transient shows a sharp drop in the initial current density due to the charging of the double layer, which was followed by a nonlinear increase in the current density with electrodeposition time. Such double layer charging was also observed during the electrodeposition of various metals [29–33]. The electrodeposition kinetics of Pd–Fe on the Au electrode in the AAO template, decreasing and then beginning to increase the current density, occurred over a very short time period. The Pd^{2+} and Fe^{2+} solutions that were used for electrodeposition filled a nanotube of the AAO template that was 5×10^6 nm^3 in volume (70 nm). To form an atomic Pd^0 and Fe^0 on the Au film at the bottom of the AAO nanotube, the process required Pd^{2+} and Fe^{2+} ions. As the required process was diffusion-controlled, double layers at the AAO nanotubes of the template could form after 30 s, which is a very short time period for this process. After forming the double layers, the continuously increasing current densities had a nonlinear characteristic.

The log(current density)–log(time) transient of increasing current density during the Pd–Fe electrodeposition on the Au electrode is shown in Fig. 4.

The slope of the log(current density)–log(time) transient in Fig. 4 is approximately 0.5 A cm^{-2} s$^{-1/2}$, which indicates that the electrodeposition kinetics follow a parabolic relationship. Therefore, the experimentally found value for the number representing the Pd–Fe nuclei density (N) can be calculated by using the following relation:

$$N = \frac{\rho^{1/2}}{zF\,\pi(2Dc)^{3/2}M^{1/2}}k_P \quad (6)$$

Here the value of the parabolic rate constant (k_P) was obtained from the slope of current density–$t^{1/2}$ transient. The electrodeposition current (I) usually obeys the following growth relation. D is the diffusion coefficient, c is the concentration of metallic ions in the solution, zF is the effective molar charge of the electrodepositing species, and t is time. M and ρ are the molecular weight and density of the metallic species deposited, respectively. We take the values of $z = 2$, $F = 96{,}500$ C mol^{-1}, $D = 6.70 \times 10^{-6}$ cm^2 s^{-1}, $M = 106.42$ g mol^{-1}, $c = 2.087 \times 10^{-6}$ mol cm^{-3}, and $\rho = 12.023$ g cm^{-3}. Thus, our Pd–Fe nanodeposition calculated value of N is 1.367×10^9.

Fig. 5 shows the SEM images of the as-deposited Pd–Fe nanowires before and after dissolving the AAO template. As shown in Fig. 5a, the Pd–Fe nanowires completely filled the AAO. Fig. 5b and c shows that the Pd–Fe nanowires are roughly parallel to each other, vertically aligned to form an array. Fabricated vertical Pd–Fe nanowires are approximately 65 nm in diameter and 10 μm in length.

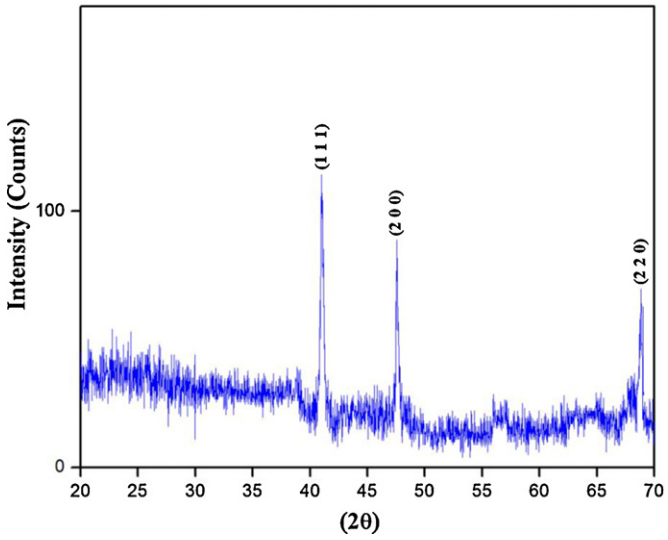

Fig. 7. XRD spectrum from the surface of the Pd–Fe nanowire array, after annealing at 500 °C.

Fig. 6 shows the EDX spectra of the as-deposited Pd–Fe nanowires. As shown in Fig. 6, the EDX spectrum from the surface of the Pd–Fe nanowire array confirms the electrodeposition process. The EDX spectra show signals from the Pd–Fe nanowires approximately at 86% of the Pd and 14% of the Fe.

Moreover, Fig. 7 shows a XRD spectrum of the Pd–Fe nanowires, after annealing at 500 °C. All of the peaks can be indexed to a (1 1 1), (2 0 0) and (2 2 0) poly-crystalline Pd–Fe with an fcc structure, indicating that Pd and Fe formed an alloy phase.

4. Conclusions

A highly ordered Pd–Fe nanowire array that has a high surface area was fabricated at room temperature by AAO template-assisted electrodeposition. The morphology, structure and growth mechanisms of these Pd–Fe nanowires were reported in detail. The initial stages of the electrodeposition of the Pd–Fe nanowires on Au were studied using potentiostat. The nucleation rate and the number of atoms in the critical nucleus are determined from the analysis of current transients. Discussions of the underlying principle that affects the properties of Pd–Fe in the present work can be helpful for further understanding the other alloy-structured nanowires. We believe that understanding the nucleation and growth mechanisms of the Pd–Fe nanowires gives rise to potential applications, especially in the field of sensors.

Acknowledgements

This study was supported by The Scientific and Technological Research Council of Turkey. The project title is “Investigation and Development of Nanotechnologic Hydrogen Sensors” and the project number is “106T546”.

References

[1] D.H. Cobden, Nature 409 (2001) 32–33.
[2] T. Goodson, O. Varnavski, Y. Wang, Int. Rev. Phys. Chem. 23 (2004) 109–150.
[3] P.V. Kamat, J. Phys. Chem. B 106 (2002) 7729–7744.
[4] S. Manalis, K. Babcock, J. Massie, V. Elings, M. Dugas, Appl. Phys. Lett. 66 (1995) 2585–2587.
[5] S.Y. Chou, M.S. Wei, P.R. Krauss, P.B. Fischer, J. Appl. Phys. 76 (1994) 6673–6675.
[6] F. Favier, E.C. Walter, M.P. Zach, T. Benter, R.M. Penner, Science 293 (2001) 2227–2231.
[7] K.T. Kim, S.J. Sim, S.M. Cho, IEEE Sens. J. 6 (2006) 509–513.
[8] E. Şennik, N. Kılınç, Z.Z. Öztürk, J. Appl. Phys. 108 (2010) 054317.
[9] Y. Konishi, M. Motoyama, H. Matsushima, Y. Fukunaka, R. Ishii, Y. Ito, J. Electroanal. Chem. 559 (2003) 149–153.
[10] I.Z. Rahman, K.M. Razeeb, M. Kamruzzaman, M. Serantoni, J. Mater. Process. Technol. 153 (2004) 811–815.
[11] O. Rabin, P.R. Herz, Y.M. Lin, A.I. Akinwande, S.B. Cronin, M.S. Dresselhaus, Adv. Funct. Mater. 13 (2003) 631–638.
[12] X.L. Fei, S.L. Tang, R.L. Wang, H.L. Su, Y. Du, Solid State Commun. 141 (2007) 25–28.
[13] C.M. Wayman, Scr. Metall. 5 (1971) 489.
[14] T. Sohmura, R. Oshima, F.E. Fujita, Scr. Metall. 14 (1980) 855–856.
[15] H. Uchida, Y. Matsumura, H. Uchida, H. Kaneko, J. Magn. Magn. Mater. 239 (2002) 540–545.
[16] K. Baba, U. Miyagawa, K. Watanabe, Y. Sakamoto, T.B. Flanagan, J. Mater. Sci. 25 (1990) 3910–3916.
[17] R.C. Hughes, W.K. Schubert, J. Appl. Phys. 71 (1992) 542–544.
[18] Y.T. Cheng, Y. Li, D. Lisi, W.M. Wang, Sens. Actuator B: Chem. 30 (1996) 11–16.
[19] L. Huang, H. Gong, D.K. Peng, G.Y. Meng, Thin Solid Films 345 (1999) 217–221.
[20] P. Kumar, L.K. Malhotra, Mater. Chem. Phys. 88 (2004) 106–109.
[21] S. Nakano, S. Yamaura, S. Uchinashi, H. Kimura, A. Inoue, Sens. Actuator B: Chem. 104 (2005) 75–79.
[22] X.M.H. Huang, M. Manolidis, S.C. Jun, J. Hone, Appl. Phys. Lett. 86 (2005) 143104.
[23] N. Taşaltın, S. Öztürk, N. Kılınç, Z.Z. Öztürk, Appl. Phys. A 97 (2009) 745–750.
[24] H.N. Hu, J.L. Chen, G.H. Wu, L.J. Chen, H.Y. Liu, Y.X. Li, J.P. Qu, Acta Phys. Sin. 54 (2005) 4370–4373.
[25] H.N. Hu, C.H. Yang, J.L. Chen, G.H. Wu, J. Magn. Magn. Mater. 320 (2008) 2305–2309.
[26] V.M. Prida, V. Vega, V. Franco, J.L.S. Llamazares, M.J. Perez, J.D. Santos, L. Escoda, J.J. Sunol, B. Hernando, J. Magn. Magn. Mater. 321 (2009) 790–792.
[27] N. Taşaltın, S. Öztürk, N. Kılınç, H. Yüzer, Z.Z. Öztürk, Appl. Phys. A 95 (2009) 781–787.
[28] N. Taşaltın, S. Öztürk, H. Yüzer, Z.Z. Öztürk, J. Optoelectron. Biomed. Mater. 1 (2009) 79–84.
[29] H. Martin, P. Carro, A.H. Creus, S. Gonzalez, R.C. Salvarezza, A.J. Arvia, Langmuir 13 (1997) 100–110.
[30] J.V. Zoval, R.M. Stiger, P.R. Biernacki, R.M. Penner, J. Phys. Chem. 100 (1996) 837–844.
[31] B. Scharifker, G. Hills, Electrochim. Acta 28 (1983) 879–889.
[32] D. Bera, S.C. Kuiry, S. Seal, J. Phys. Chem. B 108 (2004) 556–562.
[33] Y. Gimeno, A.H. Creus, P. Carro, S. Gonzalez, R.C. Salvarezza, A.J. Arvia, J. Phys. Chem. B 106 (2002) 4232–4344.